Spin-1 Centers in Neutron-Irradiated Silicon*

Wun Jung† and G. S. Newell

Department of Physics, Purdue University, Lafayette, Indiana

(Received 15 April 1963)

Electron paramagnetic resonance was used to study a number of fast-neutron-induced defects formed in pile-irradiated silicon and to follow their concentrations as a function of annealing. Measurements were made at 300, 77, and 4.2°K on samples which had attained intrinsic resistivity during irradiation, using superheterodyne spectrometers operating at 24 and 9.4 kMc/sec. Aside from the previously reported Si-N center, the most prominent lines of the spectrum arise from the $m_s = 0$ to ± 1 transitions of four spin-1 systems. The distinct symmetry and small production rate (≈ 0.05 center per fast neutron collision) indicate a class of well-defined but relatively rare defects. Their g tensors, zero-field splitting tensors, and hfs are compatible with systems having two weakly interacting $\langle 111 \rangle$ dangling bonds separated by about 5 Å, giving the $S=1$ Hamiltonians in the triplet levels formed by the weak exchange interaction. Low-temperature measurements suggest that the singlet-triplet splitting lies between 3 and 50 cm^{-1}. Comparison with floating-zone silicon shows Center (II, III), which is dominant in unannealed samples, to be independent of impurity. The remaining three $S=1$ centers, which grow and decay rapidly at higher temperatures, involve oxygen. Precise measurements of the parameters of the spin Hamiltonians are given to permit reproducible identification of the centers.

I. INTRODUCTION

SINCE the electron paramagnetic resonance (EPR) of the radiation induced defects in neutron irradiated silicon was first reported by Schultz-Du Bois and co-workers,[1] the EPR study of neutron irradiated silicon has been extended by Nisenoff and Fan,[2] who made a detailed investigation of the Si-N center which accounts for the simplified spectra after partial annealing. The EPR study of electron irradiated silicon has been made by Bemski,[3] and by Watkins and Corbett[4-8] in greater detail. Watkins and Corbett have identified several EPR centers and their detailed microscopic structures. The EPR spectra are believed to arise from an unpaired electron in a "broken bond" orbital associated with a lattice vacancy either alone or in a trapped or agglomerated state. In the case of fast neutron irradiation, more complex defect centers are expected. The well-resolved EPR spectra reported here, however, arise from well defined structures and probably represent a class of rather simple but relatively rare defects.

Some of the important factors in radiation effect studies are: (1) The temperature of the sample during irradiation, which, among other things, controls the diffusion of the mobile defects (vacancies) and affects the defect configuration to some extent; (2) the energy of the bombarding particles, which would give information on the threshold energy to produce a particular type of defect; and (3) the Fermi level of the sample, which above all determines whether a given defect will be in a charge state which is paramagnetic. We have not yet attempted to vary these factors in a systematic manner. The temperature and the energy spectrum of the neutron flux depended on the reactor used. Regardless of its initial value, the resistivity of the samples invariably approached the intrinsic value of 10^5 Ω-cm after irradiation to an integrated fast flux exposure of 10^{17} to 10^{19} *nvt*. The Fermi level is locked near the middle of the forbidden gap and remains there up to an annealing temperature of 450°C. Thus, the present study is confined to those intrinsic or oxygen containing defects which at room temperature give rise to EPR spectra near the free electron g value. Those defects which assume paramagnetic charge states only when the Fermi level is nearer one of the band edges are excluded, even though some, such as the Si-A center, are probably present in substantial concentrations.

The four spin-1 centers reported here, together with the Si-N center, account for the most prominent of the complex spectra observed at various stages of annealing.

II. EXPERIMENTAL PROCEDURE

The silicon samples studied are listed in Table I. Their initial resistivities before irradiation ranged from 0.2 to 11 000 Ω-cm. After fast neutron irradiation to a total exposure of 10^{17} to 10^{19} *nvt*, the resistivities all approached the intrinsic value of 10^5 Ω-cm. Sample 1 was irradiated in the CP-5 reactor of the Argonne National Laboratory at a temperature of about 100°C. The observed EPR spectra clearly showed the effect of slow annealing in the reactor during the irradiation. Samples 2, 3, and 4 were irradiated in the graphite reactor of the Oak Ridge National Laboratory at about 50°C. An

[1] E. O. Schultz-DuBois, M. Nisenoff, H. Y. Fan, and K. Lark-Horowitz, Phys. Rev. 98, 1561 (A) (1955).

[2] M. Nisenoff and H. Y. Fan, Phys. Rev. 128, 1605 (1962).

[3] G. Bemski, J. Appl. Phys. 30, 1195 (1959).

[4] G. D. Watkins, J. W. Corbett, and R. M. Walker, Bull. Am. Phys. Soc. 4, 159 (1959).

[5] G. D. Watkins and J. W. Corbett, J. Appl. Phys. 30, 1198 (1959).

[6] G. D. Watkins and J. W. Corbett, Phys. Rev. 121, 1001 (1961).

[7] G. D. Watkins and J. W. Corbett, Discussions Faraday Soc. 31, 89 (1961).

[8] G. D. Watkins and J. W. Corbett, Phys. Rev. Letters 7, 314 (1961).

Table I. List of samples.

Designation	Bomb'd	Flux (nvt)	Impurity	Original resistivity (Ωcm)	Bomb's temp (°C)	Centers observed[a]
1. West D-110G (crucible grown)	ANL	1×10^{19}	As, 10^{15} cm^{-3}	0.2 to 0.5	100	N, (I,I′), (V,VI), (VII,VIII)
2. USSC No. 4 (crucible grown)	ORNL	1.4×10^{18}	Residual B	131	50	(II,III), N, (I,I′), (V,VI), (VII,VIII), IX
3. Merck A65-24A (vac floating zone)	ORNL	1.2×10^{18}	Residual B	11 000	50	(II,III), IX, N
4. Merck C890-30B (vac floating zone)	ORNL	1.8×10^{18}	Residual B	3300	50	(II,III), IX, N

[a] See Fig. 5 for details of the heat treatments.

extensive isochronal annealing study was made on sample 2 and the growth and decay of the EPR centers were investigated. Samples 3 and 4 are vacuum floating-zone crystals and were used to study the oxygen dependence of the centers.

The total fast neutron flux of each Oak Ridge irradiation was calibrated using the 1.8 μ band absorption of the control sample included in the irradiation. The absorption coefficient of the 1.8 μ band increases linearly with the total fast neutron flux in the range of 10^{17} to 2×10^{18} nvt, and has a proportionality constant of 41.3 ± 0.5 cm^{-1} per 10^{18} nvt.[9] The integrated exposure thus calibrated was consistent within 10% with the value supplied by the Oak Ridge National Laboratory and defined by the comparative rates of electron removal in germanium, resistivity change in copper, and precipitation hardening experiments on alloys.[10] The 1.8 μ absorption band, however, is very sensitive to annealing and cannot be used with the higher temperature Argonne irradiations where a discrepancy of as much as a factor of 10 is sometimes found. The total exposure of 10^{19} nvt quoted for sample 1 is the nominal value given by the Argonne National Laboratory.

A superheterodyne EPR spectrometer operating at 24 kMc/sec was built for the present study. Its essential parts consist of a reflection sample cavity and three sets of balanced mixers, each followed by a 25 Mc/sec i.f. preamplifier and an i.f. demodulator. The first channel served to phaselock the local oscillator to the main klystron with a frequency offset of 25 Mc/sec; the second to stabilize the main klystron frequency to an external reference cavity; and the third to detect the EPR signal. Magnetic field modulation and lock-in detection at 500 cps were employed. A similar superheterodyne spectrometer was used for X band (9.4 kMc/sec) measurements.

The sample cavity was a TE_{102} mode rectangular cavity containing a quarter wavelength sample slab chosen to give an optimum filling factor. A tiny piece of ruby crystal (1.79 mg with 0.1% Cr^{3+}) was mounted on the end wall opposite the sample as an internal intensity standard. From the known field configuration,

the relative amplitudes of the EPR signals could be converted to absolute spin concentrations.

Except for the low-temperature measurements discussed in Sec. IV E, all EPR measurements were made in the absorption mode at room temperature.

A Varian Associates 12-in. electromagnet with a 2.125-in. gap supplied the external magnetic field, which was rotated through 90° in a (110) plane of the crystal to include the three simple crystallographic directions, $\langle 100 \rangle$, $\langle 111 \rangle$, and $\langle 110 \rangle$. The exact location of the $\langle 100 \rangle$ axis was determined by preliminary resonance measurements and the relative azimuth of the magnetic field was measured to $\pm 0.1°$.

By measuring the microwave and proton resonance frequency with the same frequency counter, the ratio of the microwave frequency to the magnetic field was determined to five significant figures, free from most systematic instrumental errors.

In a normal run, spectra were taken at 10° intervals of the magnetic field orientation. For critical runs the interval was cut to 2°. Thus each run consisted of 11 to 46 recorder traces. To facilitate analysis, the observed positions of the resonance lines were plotted against the angular displacement of the magnetic field.

III. HAMILTONIANS

The EPR spectra of the spin-1 centers with which we are primarily concerned can be described by the spin Hamiltonian

$$\mathcal{H} = \beta \mathbf{H} \cdot \mathbf{g} \cdot \mathbf{S} + \mathbf{S} \cdot \mathbf{D} \cdot \mathbf{S} + \Sigma_j \mathbf{I}_j \cdot (\mathbf{A}_j \cdot \mathbf{S} + \mathbf{B}_j \cdot \mathbf{H}), \quad (1)$$

with $S = 1$. The first term gives the Zeeman interaction of the electron spin with the external magnetic field and includes the anisotropic g shifts. The second, or zero-field splitting term, is frequently written in terms of the principal values of the D tensor in the form

$$\mathbf{S} \cdot \mathbf{D} \cdot \mathbf{S} = D[3S_z^2 - S(S+1)] + E(S_x^2 - S_y^2), \quad (2)$$

where

$$D = \tfrac{1}{2} D_{zz}, \quad E = \tfrac{1}{2}(D_{xx} - D_{yy}), \quad \text{and} \quad \text{tr}\mathbf{D} = 0.$$

The third term describes the hyperfine interaction of the electron spin with nearby Si^{29} nuclei (4.7% abundant, $I = \tfrac{1}{2}$) and the direct interaction of the nuclear spins

[9] M. Nisenoff, Semiconductor Research, First Quarterly Report, Purdue University 1956, p. 27. Contract DA 36-039-sc-71131 (unpublished).

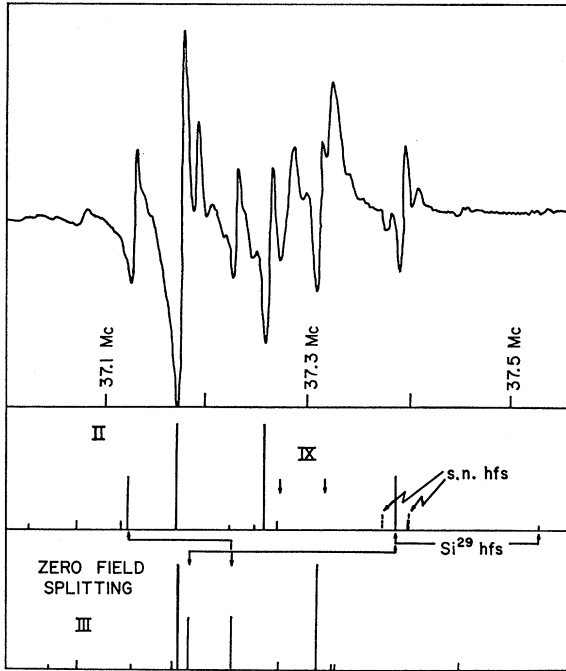[10] J. W. Cleland (private communication).

Fig. 1. EPR spectrum of center (II,III) with $H\|\langle110\rangle$. Sample 4 (vacuum-floating-zone silicon, $\phi=1.8\times10^{18}$ nvt at ORNL) annealed at 100°C for 30 min. $T=300°K$, $\nu=24.552\,108$ kMc/sec. The principal lines are marked according to whether they belong to Set II or Set III. The hyperfine satellites (5.1% relative amplitudes) due to the Si^{29} nuclei in the nearest lattice sites and the close-spaced satellites (23.6% relative amplitudes) due to those in next nearest sites are visible on one of the isolated branches.

with the external field. In general, $\mathbf{g}$ and $\mathbf{D}$ are tensors which reflect the overall symmetry of the electronic wave function, while the hyperfine tensors, $\mathbf{A}_j$, are sensitive to the details of the wave function in the vicinity of the jth nucleus. The direct nuclear Zeeman interactions represented by the tensors $\mathbf{B}_j$ are unresolved in our data and will be neglected.

Because of the low abundance of Si^{29}, the strong lines of the spectrum are given by setting the nuclear terms to zero, corresponding to Si^{28} in the nearby lattice sites. It is, thus, convenient to treat the fine structure resulting from the electronic terms of the Hamiltonian first, reserving the discussion of the weaker hyperfine satellites structure for a later section.

The energy levels of the Hamiltonian

$$\mathcal{K}=\beta\mathbf{H}\cdot\mathbf{g}\cdot\mathbf{S}+\mathbf{S}\cdot\mathbf{D}\cdot\mathbf{S} \qquad (3)$$

are obtained in the Appendix by treating the zero-field splitting as a perturbation. For a given orientation of the external field we define the effective g value, $g_e=[\mathbf{n}\cdot\mathbf{g}^2\cdot\mathbf{n}]^{1/2}$, and the effective zero-field splitting, $D_e=\mathbf{k}\cdot\mathbf{D}\cdot\mathbf{k}$, where $\mathbf{n}=H^{-1}\,\mathbf{H}$ is the unit vector in the direction of the external field and $\mathbf{k}=|\mathbf{g}\cdot\mathbf{n}|^{-1}\mathbf{g}\cdot\mathbf{n}$ is the unit vector in the direction of the effective field seen by the electron. For $S=1$ the transition frequencies are

given by the expression

$$m_s=0 \text{ to } \pm1: \quad h\nu_\pm=g_e\beta H\pm\tfrac{3}{2}D_e$$
$$+(4g_e\beta H)^{-1}(\mathrm{tr}\mathbf{D}^2-\tfrac{3}{2}D_e^2), \qquad (4)$$

where $\mathrm{tr}\mathbf{D}=\Sigma_iD_{ii}=0$ and $\mathrm{tr}\mathbf{D}^2=\Sigma_{ij}D_{ij}^2$.

For reasons of experimental convenience the transitions are observed at constant frequency by varying the magnetic field. Let H_+, H_- denote the fields at which the $m_s=0$ to ±1 transitions are observed at the given microwave frequency, ν, and let $\bar{H}=\tfrac{1}{2}(H_++H_-)$. Then Eqs. (4) may be solved consistently to give

$$\mathbf{n}\cdot\mathbf{g}^2\cdot\mathbf{n}=g_e^2=(h\nu/\beta\bar{H})^2[1-\tfrac{1}{2}(h\nu)^{-2}(\mathrm{tr}\mathbf{D}^2-\tfrac{3}{2}D_e^2)], \quad (5a)$$

$$\mathbf{k}\cdot\mathbf{D}\cdot\mathbf{k}=D_e=-\tfrac{1}{3}h\nu(H_+-H_-)/\bar{H}, \qquad (5b)$$

where in each equation the errors are given by a factor $[1+O(\epsilon^4)]$, with $\epsilon\approx(D_e/g_eH)$. The quantities g_e^2 and D_e are quadratic forms in the direction cosines of the unit vectors and, thus, show the usual $\cos^2\phi$ variation when plotted against the azimuth angle, ϕ, of the external field relative to one of the crystal crystallographic axes.[11] It is from such angular variation plots that the tensors $\mathbf{g}$ and $\mathbf{D}$ are determined. In the silicon centers the procedure is somewhat simplified by the fact that the second-order terms in Eq. (5a) are very small and need be included only in the final adjustment of the g tensor.

IV. EXPERIMENTAL RESULTS

A. Anisotropy of the Fine Structure Spectrum

Under conditions of random bombardment, a given defect of low symmetry will be produced with equal probability in any of the 48 equivalent orientations generated by the point group (O_h) of the silicon lattice. The number of distinct lines in the EPR spectrum which represent a single transition is reduced to 24 by the invariance of the Hamiltonian under inversion, and to 12 by confining the external field to a (110) plane of symmetry. Any special symmetry of the defect may still further reduce the complexity of the spectrum; in particular, all the EPR centers so far reported in silicon have Hamiltonians in which at least one axis of each of the tensors lies along $\langle110\rangle$. In the absence of additional symmetry, a plot versus external field orientation of the fine structure representing a single transition in such a defect consists of 7 branches, 5 of which have double intensity. Among these branches there exist several relations which serve as criteria of the consistency of the assignment of the resonances to the set representing a

---

[11] Strictly speaking, D_e varies as $\cos^2\phi'$, where ϕ' is the azimuth of the effective magnetic field given by the unit vector $\mathbf{k}$ rather than by $\mathbf{n}$. For the g tensors observed here, the maximum angle between $\mathbf{k}$ and $\mathbf{n}$ is of the order of $\tfrac{1}{2}(g_{ii}-g_{jj})/g_{ii}\approx0.0025$ rad $\approx0.15°$, and the distinction is neglected. A quantity which varies rigorously as $\cos^2\phi$ is $(g_e/g_0)^2D_e=g_0^{-2}\mathbf{n}\cdot\mathbf{g}\cdot\mathbf{D}\cdot\mathbf{g}\cdot\mathbf{n}$, where g_0 is any convenient number. Thus, if the g tensor is strongly anisotropic the usual curve-fitting procedures should be used to determine the tensor $g_0^{-2}\mathbf{g}\cdot\mathbf{D}\cdot\mathbf{g}$, from which $\mathbf{D}$ itself can be derived.

TABLE II. Spin Hamiltonians (300°K). $\mathcal{H}=\beta H\cdot g\cdot S+D[3S_z^2-S(S+1)]+E(S_x^2-S_y^2)$: $D=\tfrac{1}{2}D_{zz}$, $E=\tfrac{1}{2}(D_{xx}-D_{yy})$.

Centers	Frequency (kMc/sec)	g_1[a]	g_2	g_3	Δg	θ	D (Mc/sec)	E (Mc/sec)[b]	$\Delta D, E$	β[c]
(I,I')	24.090 296	2.0098_9	2.0091_2	2.0023_1	$\pm0.0000_5$	37.2°	-102.83	-16.82	±0.19	8.3°
	9.366 163	2.0098_2	2.0087_8	2.0020_4	$\pm0.001_4$	37.0°	-103.09	-15.79	±0.31	8.3°
(II,III)	24.112 101	2.0101_8	2.0099_4	2.0009_6	$\pm0.0000_6$	34.4°	-22.82	0.46	±0.12	$-6.3°$
	9.397 429	2.0102_9	2.0099_5	2.0009_3	$\pm0.0000_4$	34.1°	-22.89	0.53	±0.08	$-6.4°$
(V,VI)	24.142 383	2.0070_5	2.0089_8	2.0042_9	$\pm0.0000_3$	$-3.5°$	-41.77	2.33	±0.07	6.1°
	9.366 163	2.0072_7	2.0089_2	2.0041_3	$\pm0.0001_8$	$-6.9°$	-41.85	1.90	±0.15	6.2°
(VII,VIII)	24.110 956	2.0072_3	2.0089_9	2.0051_0	$\pm0.0001_5$	0.0°	-45.87	-1.62	±0.12	0.0°
	9.318 325	2.0072_2	2.0090_9	2.0050_1	$\pm0.0001_5$	0.0°	-45.44	-0.35	±0.34	0.0°
N	24.142 383	2.0089_9	2.0125_0	2.0046_0	$\pm0.0000_4$	17.3°	$S=\tfrac{1}{2}$			
	9.366 163	2.0090_1	2.0125_6	2.0044_5	$\pm0.0004_5$	17.5°				

[a] g_2 is along $\langle110\rangle$; g_1 lies in the plane containing $\langle001\rangle$ and $\langle\bar{1}10\rangle$, making an angle θ with $\langle001\rangle$. See Fig. 3.
[b] The sign of E is relative to D. The absolute signs are undetermined.
[c] β =angle between the x axis and $\langle001\rangle$. The sign is relative to θ.

single transition.[12] In particular, the crossing of these branches in the $\langle001\rangle$ orientation gives two lines of relative intensity 4:8; in the $\langle111\rangle$ orientation, three lines in the ratio 3:3:6, and in the $\langle110\rangle$ orientation, four lines, 2:4:4:2.
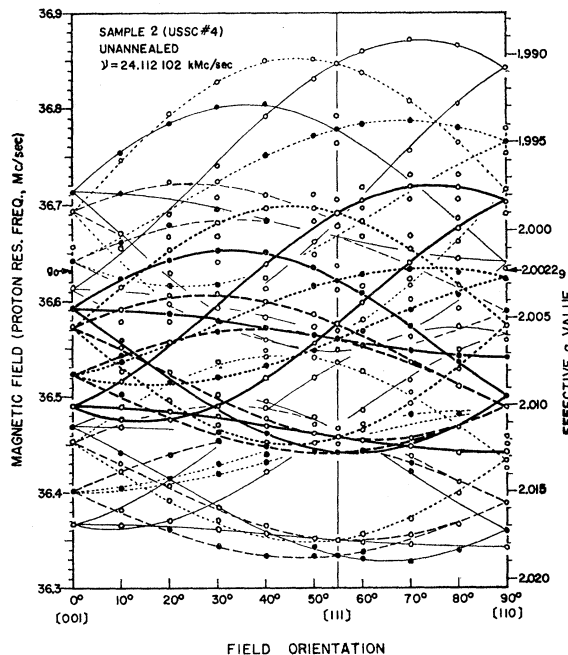

FIELD ORIENTATION

FIG. 2. Angular variation plot of center (II, III) spectrum. Sample 2 (crucible-grown silicon, $\phi=1.4\times10^{18}$ nvt at ORNL), unannealed. $T=300°K$, $\nu=24.112$ 101 kMc/sec. The external magnetic field, shown in proton resonance frequency (Mc/sec), is rotated in a (110) plane. The open circles belong to Set II and the closed circles to Set III. The diameter of the circles corresponds to the full width between inflections of the resonance lines. The thick lines represent the fine structure lines and the thin lines the hyperfine satellite lines. The branches are coded by solid, dashed, and dotted lines to indicate the pairs belonging to the same orientation of the center. The second-neighbor hfs lines are also shown on two upper branches of Set II.

[12] The consistency relations together with convenient methods for fitting the Hamiltonians will be discussed in another paper.

Figure 1 shows the EPR spectrum of center (II,III) [13] in the $\langle110\rangle$ orientation. The two transitions, $m_s=0$ to ±1, give rise to two sets of four lines. In Fig. 1 the lines are labeled II or III, according to the transition to which they belong.

Figure 2 is an experimental plot of all the lines observed in the spectrum of Center (II,III). The light curves are hyperfine satellites and will be discussed later. The 14 heavy curves representing the fine structure are coded with open or closed circles to indicate the set to which they belong.

B. Experimental Hamiltonians

The experimentally determined parameters of the Hamiltonians for the spin-1 centers and for the N
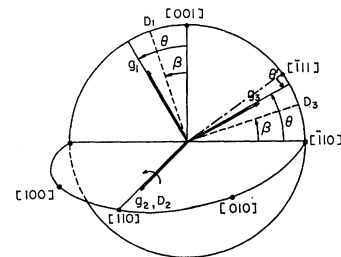
FIG. 3. Principal axes of the g and D tensors. The principal axes of the A tensors are defined in the same manner. By replacing θ by $(35°16'-\theta)$, this system can be converted to that adopted by Watkins and Corbett (Refs. 4–8). In the latter system, however, one must specify whether the 1 axis lies closer to $\langle001\rangle$ or to $\langle110\rangle$. The sign of β is relative to θ. The absolute signs are irrelevant.

[13] Our nomenclature requires a few remarks. In parallel with the terminology adopted by Watkins and Corbett, and by Nisenoff and Fan, we propose to designate the $S=\tfrac{1}{2}$ centers as Si-IX, and so on, to specify explicitly that the centers are observed in silicon. Since it is clear that this paper refers only to silicon, we will refer to them as center IX, etc. In the preliminary reduction of this data the sets of resonances belonging to the two transitions of the $S=1$ centers were separately identified and named. [See W. Jung and G. S. Newell, Bull. Am. Phys. Soc. 7, 186 (1962).] As it is sometimes convenient to refer to these sets separately, we have retained the compound names; Si-(II, III), or center (II, III), for example. If centers having spins greater than 1 are ever isolated, this luxury will have to be abandoned.
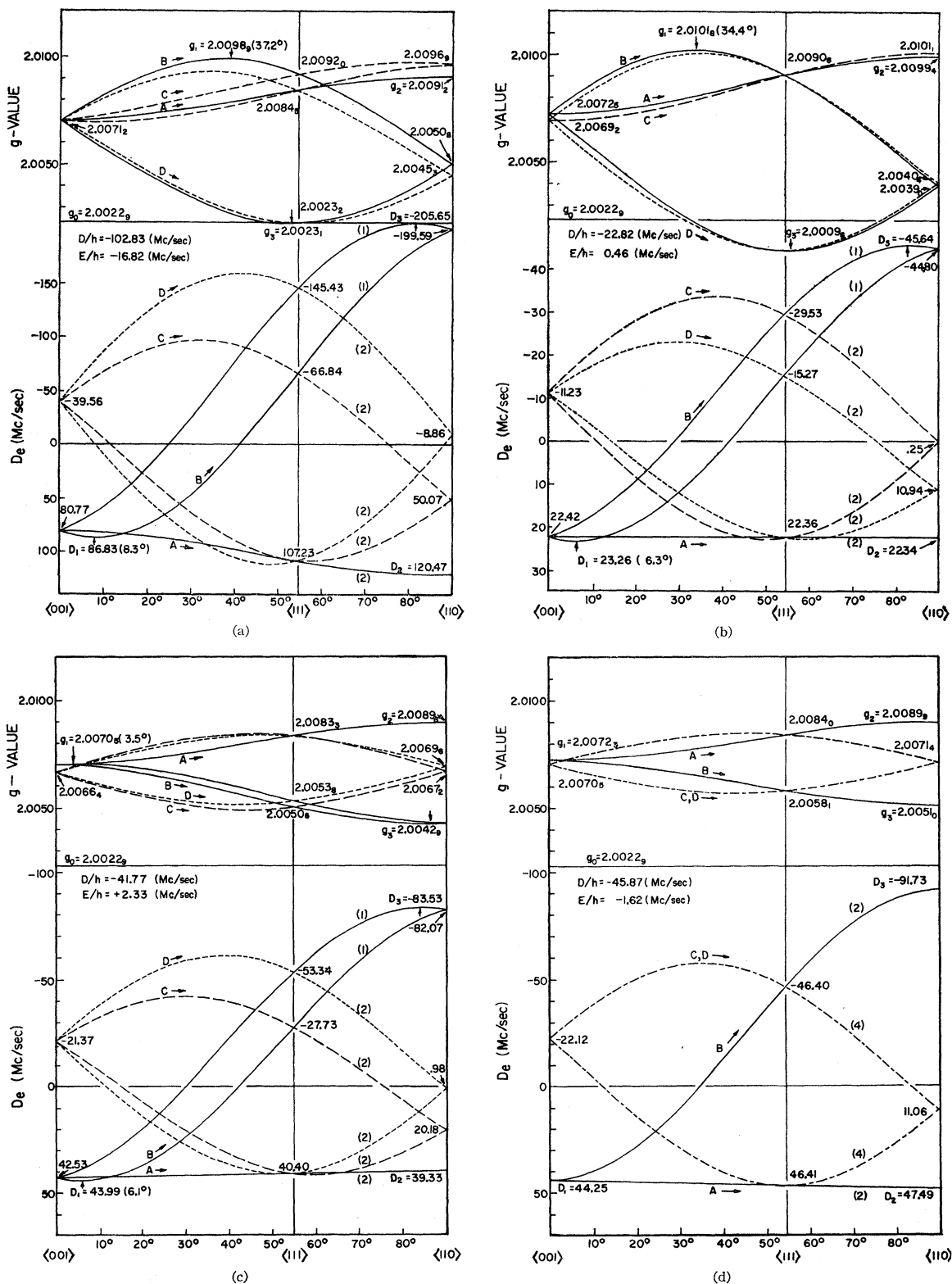
Fig. 4. Angular variation of the effective g values and zero-field splittings at 300°K. (a) Center (I,I'), (b) center (II,III), (c) center (V,VI), and (d) center (VII,VIII). At a given microwave frequency, ν, the positions of the sets of lines are given by $H = (h/g_e\beta)[\nu(1-\epsilon)+\frac{3}{2}D_e]$; $\epsilon = \nu^{-2}(\frac{1}{4}\,\mathrm{tr}\mathbf{D}^2 - \frac{3}{8}D_e^2)$, where g_e and D_e are taken from the corresponding branches at a given angle. The correction term, ϵ, is less than 2×10^{-6} for center (II,III), and less than 3×10^{-5} for center (I,I') at K band and can be neglected for most purposes.

center are tabulated on a consistent basis in Table II. Our choice of coordinate axes is specified in Fig. 3.

To obtain accuracy sufficient to permit reliable identification in the crowded EPR spectra of the lines belonging to these centers, the tabulated parameters have been adjusted by a least-squares procedure. A tensor having a $\langle 110 \rangle$ axis has at most 4 independent elements, so the total of 9 distinct values which are observed in the three simple orientations provide an over-determined set which has proved especially convenient for the adjustment. The nine values are read from angular variation curves fitted by eye and, hence, represent all the data, while the displacements caused by overlapping lines are not entirely random, so it is unlikely that a more elaborate treatment would yield greater accuracy. The tabulated mean residuals are a fair measure of the accuracy with which the relative positions of two lines will be reproduced, and in fact curves calculated from these Hamiltonians fit our data to ± 0.5 G, or one-fourth to one-half linewidth. The fit is illustrated in Fig. 2, in which the curves are calculated and the diameter of the data points is equal to the linewidth. Making allowance for possible systematic errors, we estimate the absolute accuracy to be ± 0.0001 in g values, ± 0.5 Mc/sec in zero-field splittings, $\pm 0.2°$ in θ, and $\pm 0.5°$ in β.

When comparing experimental data it is inconvenient to calculate the position of each resonance line directly from the corresponding spin Hamiltonian. Figures 4(a) to (d) show the angular variation of the effective g values and zero field splittings, g_e and D_e, respectively, as the magnetic field is rotated in the (110) plane. If ν is the microwave frequency, the resonance fields for the $m_s = 0$ to ± 1 transitions are given by

$$H = (g_e\beta)^{-1}h[\nu(1-\epsilon)\pm\tfrac{3}{2}D_e],$$

$$\epsilon = \nu^{-2}[\tfrac{1}{4}\,\mathrm{tr}\mathbf{D}^2 - \tfrac{3}{8}D_e^2],$$

where g_e and D_e are taken from corresponding branches at the given angle. To save clutter, the proper correspondence has been established by coding the lines: For example, two solid lines correspond if each crosses a dotted line in the $\langle 111 \rangle$ direction. Where ambiguity exists, the branches have been lettered. Selected values of g_e and D_e are noted, together with the corresponding values of ϕ where appropriate. The numbers in parentheses indicate the relative intensities. At K band the maximum value of ϵ varies from 2×10^{-6} for center (II,III) to 3×10^{-5} for center (I,I′), and the correction term can be neglected for most purposes.

C. Frequency Dependence

For the $S = 1$ centers, Eqs. (5a) and (5b) show that the quadratic forms, g_e^2 and D_e, are quite different functions of the two resonant fields, H_+ and H_-, which characterize the two transitions belonging to a center in a given orientation. In principle, only these functions should give consistent $\cos^2\phi$ plots, but in practice the

anisotropies and zero-field splittings observed in silicon are so small that spectra observed at a single frequency can with equal consistency be interpreted as arising from one $S = 1$ system or from two independent $S = \tfrac{1}{2}$ systems. The correct interpretation is established by correlating the two sets of branches in pairs which show frequency-independent field splittings. This correlation is necessary if the quantities $\bar{H}$ and $(H_+ - H_-)$ are to be formed correctly, and is unique except that additional information is required to assign m_s values and hence to determine the over all sign of $\mathbf{D}$.

The excellent agreement of the K-band and X-band parameters presented in Table II demonstrates the frequency independence of the Hamiltonians and verifies the spin assignments. In contrast, the apparent g tensors which may be constructed for the $m_s = 0$ to ± 1 transitions separately show drastic changes with frequency. That for "center II," for example, shows the smallest change, yet g_3 shifts by 0.0080 from 1.9974_2 at 24.1 kMc/sec to 1.9893_7 at 9.4 kMc/sec. The discrepancy of 0.0080 is about 100 times experimental error. The effect is much more pronounced for "centers" V, VI, I, and I′.

D. Isochromal Annealing

Growth and Decay Curves

Sample 2 (USSC No. 4, crucible grown, ORNL irradiation at $T \approx 50°C$, $\phi = 1.4\times10^{18}$ nvt) was carried through an isochronal anneal in the following steps: 90 to 170°C in 10°C steps for 30 min; 170 to 185°C in 5°C steps for 30 min; and 200 to 500°C in 50°C steps for 60 min each. The heat treatments were carried out in a high-vacuum quartz furnace.

After each step of annealing, a complete measurement of the angular variation of the EPR spectra at room temperature was made. The Q of the sample cavity remained high through steps 0 to 17 (400°C) indicating that the Fermi level remained in the middle of the forbidden gap, as expected from previous work. The Q decreased somewhat after step 18 (450°C), and quite appreciably after step 19 (500°C), at which point only unanalyzable traces of resonance remained. The centers formed at or below 400°C are thus characteristic of the intrinsic material. The room-temperature resistivity after the 500°C annealing, however, is still of the order of 10^5 Ω-cm and indicates only a slight shift in the Fermi level.

In the observed spectra resonance lines overlapped more often than not, making amplitude comparisons difficult. Using the angular variation plot for each run, all the lines which appeared in the clear at each angle were picked out for amplitude measurement, giving 15 to 40 values for each set and temperature.

To verify that the branches assigned to a single transition did in fact grow and decay together, separate annealing curves were constructed for each branch.[14] For

---

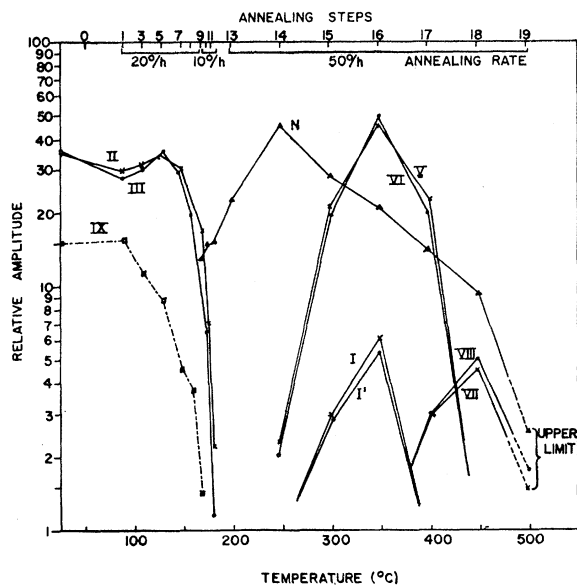[14] The branches of center (I, I′) are so clearly visible in the data that this test was unnecessary.

FIG. 5. Isochronal annealing curve. Sample 2 (crucible grown, $\phi=1.4\times10^{18}$ at ORNL). The mean EPR amplitudes at 300°K for each set of lines belonging to a single transition are plotted versus annealing temperature. The pairs of curves belong to the $m_s=-1$ to 0 and $m_s=0$ to $+1$ transitions of the $S=1$ centers. The annealing steps are: 90 to 170°C in 10°C steps for 30 min each; 170 to 185°C in 5°C steps for 30 min; and 200 to 500°C in 50°C steps for 60 min each. The ordinate is the amplitude of a single branch of unit multiplicity relative to 100 for the $-\frac{1}{2}$ to $+\frac{1}{2}$ transition of Cr^{+3} in the internal ruby standard. For estimates of the absolute concentrations, see Table III.

a given run, the branches belonging to a set showed a maximum spread of 2:1 in amplitude (after taking the expected multiplicity of each branch into account), with a standard deviation of 16% from the mean. As several sets were followed over a 20:1 variation in concentration, the agreement is convincing.

Figure 5 plots the annealing behavior of the mean amplitude of each of the sets of lines. The parallel growth and decay curves of the pairs of sets belonging to the spin-1 centers is striking and fully confirms the field dependence studies. The standard deviation of each point lies between 5 and 10% and is less than the apparent systematic variation of 15% observed in the annealing curves of Sets II and III below 130°C[15]: Each curve is, therefore, self-consistent to ±20%.

The spin Hamiltonians of the N center and the four $S=1$ centers have been discussed above. Center IX of Fig. 5 consists of three lines which anneal together and which do not belong to any of the other centers. They show a weak angular variation and are obscured at most angles by center (II,III): The visible portions are correctly described at 24 kMc/sec by a g tensor with apparent g values of 2.0009, 2.0032, and 2.0054 (±0.0003) along the three ⟨100⟩ directions. Aside from the annealing data, this center is established principally

[15] This variation may be real or may result from small changes in the relative filling factors of the ruby standard and the sample when the latter is replaced after each run.

by elimination, and it is quite possible that its high symmetry is illusory.

Figure 5 also clarifies the relation between Oak Ridge ($T\approx50°C$) and Argonne ($T\approx100°C$) irradiations. The N center and Set I were originally observed in unannealed Argonne irradiated material containing arsenic (sample 1), the rest of the very complex spectrum being uninterpretable. After isolating centers, (I,I′), (V,VI), and (VII,VIII), however, we have identified all the important lines in the Argonne sample and find the relative defect concentrations to correspond roughly to those in the pure Oak Ridge material annealed to a temperature between 300 and 350°C, thus demonstrating the effects of slow annealing in the pile.

Centers (II,III) and IX account for the entire room temperature spectrum up to the 180°C stage of annealing. This is illustrated in Fig. 2, which actually plots every resonance observed. The few points which do not lie on branches calculated for center (II,III) belong either to the next-nearest-neighbor hfs, or to center IX.

At higher annealing temperatures, the centers in Table II and Fig. 5 account for the most prominent lines of the spectrum; however at each stage perhaps one or two additional centers are present and give as yet unidentified lines having amplitudes up to 30% of the main ones. In particular, there are some indications that a complex sequence of rearrangement sets in above 400°C, possibly in connection with the coagulation of oxygen. Some of the unidentified lines are broad and represent substantial defect concentrations. They are heavily obscured and it remains to be seen whether further experiments will disentangle them.

Defect Concentrations

Assuming the same line shape (Gaussian) and identical experimental conditions, the relative concentration of two centers is given by

$$N_1/N_2=A_1(\Delta H_1)^2/A_2(\Delta H_2)^2,$$

where A_i is the amplitude relative to the internal standard and ΔH_i the line width. The 20% uncertainty in ΔH introduces an uncertainty of 1.4:1 in the concentrations. Further, the amplitude of the hyperfine satellite lines must be added to that of the main lines. This correction amounts to about 57% for center (II,III), but has not been applied in Fig. 5 as the hyperfine satellites of the other centers are less certain. The annealing curves of the figure, therefore, show only the relative amplitudes of the fine structure lines of various centers.

From the amplitude of a center relative to that of the internal ruby standard, its absolute concentration can be estimated using the relation

$$n_s=\frac{N_s}{V_s}=N_r\frac{\eta_r\alpha_rC_sA_s(\Delta H_s)^2}{\eta_s\alpha_sC_rA_r(\Delta H_r)^2}\frac{12}{V_s}$$

$$=5.25\times10^{15}\frac{(\Delta H_s)^2}{\alpha_s}\frac{A_s}{A_r},$$

TABLE III. Concentrations of EPR centers in neutron-irradiated silicon. Sample 2 (USSC No. 4, $\phi=1.4\times10^{18}$ nvt, ORNL).

Centers	S	ΔH (G)	A_s/A_r	n (10^{15} cm^{-3})	Corrections (%) hfs	singlet	Final (10^{16} cm^{-3})	Impurity dependence
(II,III)	1	1.2	0.359	4.07	+57	+33.3	0.85	independent
IX	$\frac{1}{2}$	1.4	0.155	3.19	unknown	$\cdots$	0.32	independent
N	$\frac{1}{2}$	1.2	0.451	6.82	+9.8	$\cdots$	0.75	independent
(I,I')	1	2.4	0.0576	2.59	unknown	+33.3	0.35	oxygen-dependent
(V,VI)	1	1.2	0.442	5.02	+50	+33.3	1.00	oxygen-dependent
(VII,VIII)	1	1.6	0.0478	0.97	+50	+33.3	0.19	oxygen-dependent

where the symbols are defined as follows:

$$\frac{\eta_r}{\eta_s}=\frac{\langle H_{rf}^2\rangle \text{ruby}}{\langle H_{rf}^2\rangle \text{sample}}=\text{the relative filling factor}=0.216.$$

$\alpha_s=$ transition probability factor

$$=\frac{S(S+1)-m_s(m_s+1)}{2S+1}.$$

$\alpha_r=1.02$ instead of 1 for the $m_s=-\frac{1}{2}$ to $+\frac{1}{2}$ transition of Cr^{3+} in ruby due to the matrix element correction.

$\Delta H_s=$ linewidth

$\Delta H_r=$ linewidth of ruby signal $=15.9$ G (full width between inflections).

$N_r=$ number of Cr^{+3} spins in 1.79 mg of ruby $\approx2.07\times10^{16}$.[16]

$V_s=$ sample volume $=1.03\times0.43\times0.093$

$=4.12\times10^{-2}$ cm^3.

$A_s/A_r=$ amplitude ratio

$C_s, C_r=$ line shape factors: $C_s=C_r$, assuming the same line shape (Gaussian).

The factor of 12 results from the fact that the amplitudes plotted in Fig. 5 are for a single branch normalized to unit multiplicity.

The peak concentrations of the centers at various stages of annealing are collected in Table III. The table includes corrections for (1) hyperfine satellite lines and for (2) singlet level populations for the spin-1 centers. For center (II,III), for example, weak satellites (4.9%) and the second-neighbor (s.n.) satellites (23.6%) give rise to $\sim57\%$ hfs correction. For centers (V,VI) and (VII,VIII), only the s.n. satellites are taken into account and, hence, the 50% correction is only approxi-

mate. For the N center, no s.n. structure was observed and the correction represents the contribution of the weak satellites alone. The singlet level population corrections for spin 1 centers were assumed to be $+\frac{1}{3}$ by taking a statistical weight of $\frac{1}{4}$ for the single levels and neglecting the Boltzmann factor.

In addition to the uncertainty in the Cr^{+3} ion concentration in the ruby standard, the scattering in line widths and the hfs corrections make these values unreliable as much as by a factor of 2. The final concentrations range from 0.2 to 1.0×10^{16} centers/cm^3. Taking the average elastic scattering cross section of silicon atoms for fast neutron flux to be $\approx3\times10^{-24}$ cm^2,[17] the number of collision events per unit volume is 2.1×10^{17} cm^{-3} for the integrated exposure of 1.4×10^{18} nvt. The production rate thus ranges from 0.01 to 0.05 centers per collision. In view of the large number of knock-ons (≈20) expected, the small value obtained for the production rate appears to be significant.

E. Low-Temperature Measurements

Preliminary measurements at 77 and 4.2°K were made to look for reorientation effects analogous to those seen in the N center, and to search for evidence of depopulation of the triplet level and thus obtain an estimate of the singlet-triplet level splitting. Some semiquantitative information on relaxation times was obtained incidentally.

Two samples were prepared from the same material as sample 1, one unannealed and showing centers (II,III) and IX at room temperature and the other annealed to 350°C and showing centers N, (V,VI), and (I,I').

At 77°K, nothing unexpected was encountered. Saturation effects were pronounced, but measurements could be made in either dispersion or absorption, and were in agreement. The spectra of centers (II,III), (V,VI), and (I,I') were only slightly altered, indicating changes which only slightly exceeded experimental error in the spin Hamiltonians, in marked contrast to the behavior of the N center spectrum which underwent the transformation reported by Nisenoff and Fan.[2]

The measurement of relaxation times by saturation is

[16] The value of 2.07×10^{16} spins in the ruby standard is calculated from the nominal concentration of 0.01% Cr^{+3}. Although it is certainly in error, it is being retained until we are better satisfied with the accuracy of our own determinations. These have been: (1) comparison of the resonance amplitude with that of a known sample of CuSO$_4\cdot$5H$_2$O, giving 1.2×10^{16} spins for the ruby, and (2) comparison of the optical absorption coefficient at selected wavelengths with those given by T. H. Maiman, R. H. Hoskins, I. I. D'Haenens, C. K. Asawa, and V. Evtuhov [Phys. Rev. 123, 1151 (1961)], giving 1.4×10^{16} spins.

[17] D. J. Hughes and J. A. Harvey, Neutron Cross Sections (BNL 325, 2nd Ed.). Compiled by D. J. Hughes and R. B. Schwartz (U. S. Government Printing Office, Washington, D. C., 1958). The total cross section, σ_T, varies from 2 to 4 b for 0.1 to 10-MeV neutrons.
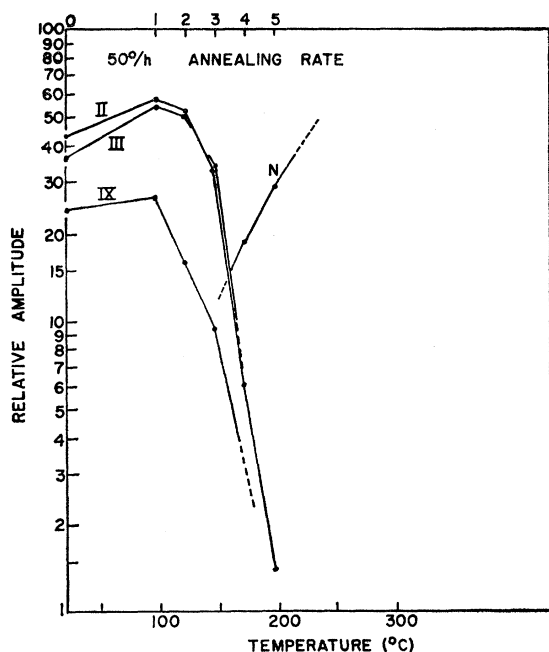
Fig. 6. Isochronal annealing curve. Sample 4 (vacuum-floating zone, $\phi = 1.8 \times 10^{18}$ at ORNL). The annealing was done in 5 steps of 25° for 30 min each, starting at 100°C. The ordinate scale is the same as for Fig. 5. The concentrations of centers (II, III), N, and IX are comparable to those for crucible-grown samples, but spot checks show the remaining centers to be absent.

rather questionable when a field modulation technique is used. Qualitatively, however, the amplitude of absorption measured at 77°K as a function of power showed that at 1 mW the N center is well saturated, while center (V,VI) shows only incipient saturation. Using Castner's method,[18] $T_1 = 2.7 \times 10^{-5}$ sec and $T_2 = 0.67 \times 10^{-6}$ sec were obtained for the N center, showing the overall line width to be about 10 times that of an individual spin packet. Because of the low degree of saturation achieved by center (V,VI), only $(T_1 T_2)^{1/2} = 0.88 \times 10^{-6}$ sec could be estimated. In the unannealed samples, when center (II,III) was well saturated, new resonance lines began to appear and prevented a reliable determination of the relaxation times. Qualitatively, however, the saturation behavior appears to be similar to that of the N center and the relaxation times are probably of the same order of magnitude.

At 4.2°K, excessive relaxation times caused a transition to a new passage case. "Derivative modulation" in dispersion gave the normal absorption profile instead of its derivative and a serious loss of resolution ensued. The derivation spectrum could sometimes be recovered by second harmonic detection. By this method the N-center Hamiltonian was shown to be substantially the same at 4.2°K as at 77°K. Comparison of the spectra at room temperature and at 4.2°K showed the spectrum of center (V,VI) to be completely absent, leaving princi-

[18] T. G. Castner, Jr., Phys. Rev. 115, 1506 (1959).

pally the N center together with some very weak lines which spread over only one half the range occupied by center (V,VI) spectra. Although experiments at intermediate temperature will be required for proof, it is probable that center (V,VI) is depopulated as expected for a triplet state.

The second-harmonic detection method has so far failed for unannealed samples, but again, the 300 and 77°K spectrum of center (II,III) is certainly absent at 4.2°K, since the spread of the unresolved lines is less than one-half that of center (II,III). We cannot, however, exclude the possibility that center (II,III) has merely reoriented.

Taking the low-temperature disappearance of the $S = 1$ spectra at face value, the exchange energy, or the triplet-singlet separation, lies between 4.2 and 77°K, or 3 to 50 cm^{-1}.

F. Oxygen Dependence

To investigate the possible oxygen dependence of the centers, samples 3 and 4 were studied. First, quick spot checks on Sample 3 were made using a condensed annealing schedule developed to achieve optimum concentrations of the higher temperature centers by simulating the 250, 350, and 450°C stages of the original annealing series. The results show the N center in approximately normal concentrations with centers (I,I'), (V,VI), and (VII,VIII) completely absent. Taking the N center as a standard, Table IV shows that the expected relative intensities are, in fact, achieved in crucible grown material, while in vacuum floating-zone material the three centers are absent and only upper limits determined by the noise level can be given.

Sample 4 was carried through an isochronal anneal starting from 100°C in steps of 25°C for 30 min each. Figure 6 plots the relative amplitude of centers (II,III), IX, and N up to 200°C on the same scale used in Fig. 5. After correcting for the slightly higher flux, the curves are in substantial agreement with those for crucible-grown material and we conclude that these three centers are independent of all impurities, including oxygen. Remodeling of the laboratory terminated the sequence at 200°C, but the result of the spot checks leads us to conclude that oxygen plays a critical role in the forma-

Table IV. Oxygen dependence of EPR centers in neutron-irradiated silicon. Amplitudes of EPR centers relative to that of the Si-N center versus simulated annealing temperature. Crucible grown silicon = Sample 2; FZ = vacuum floating zone silicon = Sample 3.

	250°C		350°C		450°C	
	Crucible	FZ	Crucible	FZ	Crucible	FZ
(V, VI)/N	0.05	<0.005	2.23	<0.01	a	...
(I, I')/N	a	...	0.28	<0.01	a	...
(VII, VIII)/N	a	...	a	...	0.50	<0.05

a Negligible.

tion of centers (I,I'), (V,VI), and (VII,VIII), and is most probably a constituent. No lines have been observed in floating-zone material which are not observed in crucible-grown samples.

G. Hyperfine Structure

For centers (II,III), (V,VI), and N, which were observed in large enough concentrations, the weak-hyperfine satellites arising from the magnetic interaction of the electronic magnetic moments with neighboring Si^{29} nuclei ($I=\frac{1}{2}$, 4.7% abundant) were observed. The recorder trace of a center (II,III) spectrum ($H\|\langle 110\rangle$) which is reproduced in Fig. 1 shows these satellites. For center (II,III), their amplitude ranges from 4 to 6% of the main lines and is well above the noise level. The separation from the center line varies from 23 to 37 G and is fairly well resolved. For centers (V,VI), and N, however, the hyperfine signals appear to be much weaker (only 2 to 3%) and are overshadowed by other centers at most angles, while the separation seems to be comparable to that of center (II,III).

In addition, some of the well-isolated branches of centers (II,III), (V,VI), and (VII,VIII) show much more closely spaced satellites (Fig. 1) arising from hyperfine interactions with the second-nearest nuclei. The lines on each side are separated from the center line by about 3 G and the amplitudes are 20 to 29% of the center lines.

The presence of several centers in each spectrum and an unfavorable signal to noise ratio prevented determination of the hyperfine tensor with any reliability except for center (II,III). Even for center (II,III) the s.n. lines were so obscured by other branches that the hyperfine tensor for those satellites was not determined.

By including the hyperfine interaction term in the spin Hamiltonian, the hyperfine satellites are described by

$$\mathcal{H}=\beta H\cdot g\cdot S+S\cdot D\cdot S+I\cdot A\cdot S$$

with $S=1$.

To first order, the energy shift due to one magnetic nucleus is

$$E(m_s,m_I)-E(m_s,0)=m_s m_I|k\cdot A|=m_s m_I A_e,$$

where $A_e{}^2=k\cdot A^2\cdot k$; m_s, m_I are the electronic and nuclear magnetic quantum numbers; and k is the unit vector in the direction of the effective field: $k=(g_e H)^{-1}g\cdot H$. As the microwave transitions correspond to $\Delta m_s=1$, $\Delta m_I=0$, the separation, ΔH, between the main and satellite lines is given by

$$g_e\beta\Delta H=m_I A_e,$$

where $m_I=\pm\frac{1}{2}$ for Si^{29}. Insertion of the parameters of center (II,III) shows the second order terms to be comparable with experimental error. Hence the hyperfine interaction tensor, A, is determined from the angular variation of the quantity

$$A_e{}^2=(2g_e\beta_0\Delta H)^2$$

Fig. 7. Hyperfine splitting of center (II, III). The separation between the hfs satellites (5.1% relative amplitude) and the corresponding branches of the fine structure is plotted versus the orientation of the external field in a (110) plane. Points taken from the $m_s=0$ to ± 1 transitions fall on the same curves and are not distinguished.

by applying the least-squares procedure developed for the fine structure tensors.

The observed and calculated angular variation of the hyperfine splitting of center (II,III) are plotted in Fig. 7. To measure a splitting, both the satellite and the main line must be visible; thus, in constructing Fig. 7, points were taken from any of the 14 main branches which happened to be usable and are keyed to the corresponding branches plotted in Fig. 2 by using similarly coded lines. For center (II,III), the following values are obtained:

$$A_1=(44.1\pm 0.4)\times 10^{-4}\text{ cm}^{-1}, \quad (\theta=36.5°\pm 0.5°)$$

$$A_2=(43.6\pm 0.4)\times 10^{-4}\text{ cm}^{-1},$$

$$A_3=(68.8\pm 0.4)\times 10^{-4}\text{ cm}^{-1},$$

where A_2 lies along $\langle 110\rangle$ and the axes are defined as usual by Fig. 3. These show a nearly axial $\langle 111\rangle$ symmetry; $A_{11}=68.8\times 10^{-4}$ cm^{-1} and $A_1\approx\frac{1}{2}(A_1+A_2)$ $=43.9\times 10^{-4}$ cm^{-1} with A_{11} lying 1.2° from $\langle 111\rangle$ toward $\langle 001\rangle$ in the (110) plane. In order to examine the over all fit of the parameters, the angular variations of the hyperfine satellite lines were calculated from the fitted values of g, D, and A, and plotted for all of the 28 hyperfine branches corresponding to the 14 main lines. Figure 2 shows the actual angular variation plot for the unannealed Sample 2. Exactly the same curves are obtained for Sample 4. The thick lines represent the 14 main lines and the thin lines the corresponding hyperfine satellites, with both the parent and satellite lines coded

in the same way as in Figs. 4(a)–(d). The fitted curves account for all of the visible portions of the hyperfine satellites within a linewidth, and as previously remarked, all the observed resonances are accounted for.

The ratio of the amplitudes of the hyperfine satellites to the main lines was measured at those angles where both lines were well isolated from others. The observed ratio of 5.12% ($\sigma=0.78\%$ from 32 measurements) is in satisfactory agreement with the value

$$[2I+1]^{-1}[_2C_1P(1-P)]/[_2C_0(1-P)^2]=0.0494$$

expected for two equivalent Si^{29} nuclei having $I=\frac{1}{2}$ and $P=0.047$, and is easily distinguishable from the values of 2.47% expected for only one nucleus, 7.42% for three, and 9.89% for four.

For a spin-1 center such as center (II,III), the orbitals localized on the two atoms overlap very slightly, giving rise to an exchange coupling. The observed hyperfine satellites correspond to the case in which only one of the two nuclei is Si^{29} ($I=\frac{1}{2}$), the other being Si^{28} ($I=0$). Within the triplet manifold, the appropriate hyperfine Hamiltonian is

$$\mathcal{3C}_{hfs}=\tfrac{1}{2}\mathbf{I}_i\cdot\mathbf{a}_i\cdot\mathbf{S}_1+\tfrac{1}{2}\mathbf{I}_i\cdot\mathbf{a}_i\cdot\mathbf{S}_2$$
$$\equiv\mathbf{I}_i\cdot\mathbf{A}_i\cdot\mathbf{S},$$

where

$$\mathbf{A}_i=\tfrac{1}{2}\mathbf{a}_i;\quad i=1 \text{ or } 2.$$

The hyperfine splitting of the energy level,

$$E(m_s,m_I)-E(m_s,0)=m_sm_I|\mathbf{k}\cdot\mathbf{A}_i|=\tfrac{1}{2}m_sm_I|\mathbf{k}\cdot\mathbf{a}_i|,$$

is exactly the same as for $S=\frac{1}{2}$, the value of $m_s=\pm1$ canceling the factor of $\frac{1}{2}$. The fact that a *single* set of satellites of 5% relative amplitude is observed indicates that $\mathbf{a}_1=\mathbf{a}_2$, and that the two nuclei are accurately equivalent. This suggests that if the distortion of the hfs axis away from $\langle111\rangle$ is due to the mutual repulsion of the dangling bonds, these bonds are antiparallel rather than parallel; in the latter case the hfs axis would differ by 2.4° and the nuclei would be clearly inequivalent.

Watkins and Corbett[6,7] discussed the hyperfine interaction of the electron irradiation centers in silicon (all $S=\frac{1}{2}$) on the following basis:

The wave function of the electron is approximated by $3s$ and $3p$ orbitals localized at various lattice sites j:

$$\psi=\sum_j\eta_j(\alpha_j\psi_{3s}{}^j+\beta_j\psi_{3p}{}^j),$$

where α_j and β_j are normalized according to $\alpha_j{}^2+\beta_j{}^2=1$. The factor $\eta_j{}^2$ gives the fractional contribution from site j, and $\alpha_j{}^2$ and $\beta_j{}^2$ give the relative weights of $3s$ and $3p$ orbitals. The values of $\eta_j{}^2$, $\alpha_j{}^2$, and $\beta_j{}^2$ can be calculated from the observed A tensor:

$$a_j=\tfrac{1}{3}(A_{\text{II}}{}^j+2A_{\perp}{}^j)=(16/3)\pi g_N\beta_0\beta_N\alpha_j{}^2\eta_j{}^2|\psi_{3s}(0)|^2,$$

$$b_j=\tfrac{1}{3}(A_{\text{II}}{}^j-A_{\perp}{}^j)=\tfrac{4}{5}g_N\beta_0\beta_N\beta_j{}^2\eta_j{}^2\langle r^{-3}\rangle_{3p},$$

where g_N is the nuclear g factor, β_0 the Bohr magnetron, and β_N the nuclear magneton. Using the value $|\psi_{3s}(0)|^2/\langle r^{-3}\rangle_{3p}=1.4$ estimated from the tabulated

Hartree functions and the value, $|\psi_{3s}(0)|^2=24\times10^{24}$ cm^{-3}, obtained from previous work on the Si-A center, the authors quoted obtain the values

$$a_j=\alpha_j{}^2\eta_j{}^2\times1040\times10^{-4}\text{ cm}^{-1}$$

and

$$b_j=\beta_j{}^2\eta_j{}^2\times36\times10^{-4}\text{ cm}^{-1}.$$

A similar analysis of the A tensor of center (II,III) gives

$$a=52.15\times10^{-4}\text{ cm}^{-1},\quad b=4.15\times10^{-4}\text{ cm}^{-1},$$

and, hence, $\alpha^2=0.176$, $\beta^2=0.824$, and $\eta^2=0.281$.

In terms of this simple model, the result is interpreted as follows: two orbitals of 18% $3s$ and 82% $3p$ character localized on two neighboring atoms account for 56% of the total wave function of each electron, the enhanced p-like character over the normal 25% $3s$ and 75% $3p$ (sp^3) tetrahedral orbital suggesting that the atom is pulled away from the normal site by its neighbors. The rest of the wave function is spread over more distant atoms.

The second-neighbor hfs lines of center (II,III) may account for a large portion of the remaining wave function. The relative amplitude varies from 20 to 29% (23.6%, $\sigma=3.7\%$ from 30 measurements), and it is difficult to distinguish among the values of 19.8% expected for eight equivalent nuclei, 24.7% for ten, and 29.7% for twelve. As the approximately ten neighboring atoms are almost certainly not equivalent for arbitrary orientations of the magnetic field, these satellites should split into groups characteristic of the structure of the center. Unfortunately, the resolution is such that the lines merely broaden and disappear. The fact they are visible over quite a range of angles reflects the small value of the coupling constant for $3p$ states.

As the hyperfine tensors for these atoms have not been determined, only rather broad limits can be placed of their contribution to the total wave function. The separations from the center lines are about 3.1 G and are nearly constant over the region where they are visible. The separation corresponds to 5.8×10^{-4} cm^{-1}. Assuming $A_\perp\approx5.8\times10^{-4}$ cm^{-1} as a reasonable guess, and assuming little disturbed normal sp^3 orbitals ($\alpha^2=0.25$ and $\beta^2=0.75$), $A_{\text{II}}=1.35\,A_\perp$, and, hence, $\eta^2\sim0.026$. Thus, by taking ten nuclei, the contribution to the total wave function amounts to 26%. However, the data are insensitive to the p component. Taking $\alpha^2=1$ as the extreme case, $\eta^2=0.006$ and the contribution to the wave function would be only 6%.

The interpretation that these close-spaced satellites arise from the interaction with a number of distant nuclei is confirmed by the occasional detection of a second pair of very faint satellites having the separations and amplitudes predicted for interactions involving *two* Si^{29} nuclei among the 8 to 12 neighbors.

The spectra of both main and hyperfine satellite lines, and their relative intensities, remain unchanged between 300 and 77°K. This suggests that the electronic

configuration is rather firmly locked and not affected in this temperature range.

In contrast, the spectrum of the N center goes through a transition at temperatures between 77 and 166°K. While the hyperfine tensor at 300°K has not been determined accurately because of an unfavorable signal-to-noise ratio, the hyperfine splitting is only one-half that of the 77°K spectra, and the relative amplitude of the satellites remains unchanged at about 2%. This suggests that at 300°K, the electronic wave function is distributed by a motional effect over two atoms which are not quite equivalent. The hyperfine interactions involving two similar but not equivalent sites should give rise to twice as many satellite lines as for two equivalent sites, each having 2.5% amplitude and comparable separations, and would make the experimental determination of the tensors much more difficult. This may very well be the case of center (V,VI) also; in fact, the anisotropy of the g tensor of the center is consistent with a pair of two $\langle 111 \rangle$ dangling bond orbitals oriented toward the center of a tetrahedron and thus supports the suggestion.

V. DISCUSSION

A. Model

The data reported here are not sufficient to establish detailed atomic models for the $S=1$ defects under consideration, but we are definitely led to a model in which the two unpaired electrons are localized in dangling tetrahedral orbitals centered on nuclei which are separated by about 5 Å, probably along $\langle 110 \rangle$.

The localization of the magnetic electrons on separate centers is indicated by the small magnitude of the zero-field splitting, and is shown conclusively for center (II,III) by the hfs. For two electrons on the same atom, Pryce's[19] treatment gives the spin-orbit contribution to the zero-field splitting in the form

$$D_{ij}=\lambda^2 \sum_{n\neq0} \frac{\langle 0|L_i|n\rangle\langle n|L_j|0\rangle}{E_0-E_n}=\lambda\frac{g_{ij}-g_0\delta_{ij}}{g_0}=\frac{\lambda}{g_0}\delta g_{ij},$$

where λ is the spin-orbit coupling constant, $g_0=2.0023$, δg is the g-shift tensor, and the trace of D has not been set to zero. For comparison with experiment it is convenient to use the quantities D and E [cf., Eq. (2)]:

$$D=\tfrac{1}{2}[D_{zz}-\tfrac{1}{3}\,\mathrm{tr}\,D]=\frac{\lambda}{2g_0}[g_3-\tfrac{1}{3}\,\mathrm{tr}\,g],$$

$$E=\tfrac{1}{2}[D_{xx}-D_{yy}]=\frac{\lambda}{2g_0}[g_1-g_2].$$

Taking $\lambda\approx0.02$ eV for silicon and inserting the g values observed for centers (II,III) and (I,I′), D is found to be approximately 2000×10^{-4} cm^{-1} for both, in contrast

[19] M. H. L. Pryce. Proc. Phys. Soc. (London) A63, 25 (1950).

to the observed values of 7.6 and 34×10^{-4} cm^{-1}. The predicted value is, thus, 50 to 250 times those observed and leads to a zero-field splitting of 0.6 cm^{-1}, which is comparable to the Zeeman splitting itself at 24 kMc/sec: $g\beta H\approx0.8$ cm^{-1}. The contribution of the direct dipole-dipole interaction should be of the same order of magnitude, as can be estimated by taking the radius of the charge cloud to be about 1 Å, but it is unlikely that the very small observed splitting could be the result of cancellation. On the other hand, if the two spins are assumed to be localized at points separated by a lattice spacing, ($a=5.42$ Å), the dipole-dipole interaction becomes

$$\left\langle \frac{\mathbf{u_1\cdot u_2}}{r^3}-\frac{3(\mathbf{u_1\cdot r})(\mathbf{u_2\cdot r})}{r^5}\right\rangle=D[3S_z^2-S(S+1)],$$

with $D\approx-27\times10^{-4}$ cm^{-1}, in agreement with the observed values. Evaluation of the spin-orbit contribution in this case requires a more careful theoretical treatment than we have attempted, but it clearly goes to zero quite rapidly as the two centers are separated, and the data are compatible only with the two-center model. As discussed below, the g tensors suggest that the electrons are localized in dangling sp^3 orbitals; if so, the dimensions of the two electron clouds are of the order of 1 to 2 Å, or substantially smaller than their separation. If the spin-orbit contribution can in fact be neglected, the D tensor should have axial symmetry, as is approximately the case, with D negative, corresponding to prolate symmetry, and with the major axis indicating the approximate line of centers. Experimentally, the sign of $\mathbf{D}$ is indeterminate, but in all cases its axis lies near to $\langle 110 \rangle$, suggesting that the separation of the two electrons also lies along $\langle 110 \rangle$.

The field dependence of the observed $S=1$ Hamiltonians is accurately linear and shows no sign of repulsion between the singlet and triplet levels formed by the interaction of the two spins. The singlet-triplet separation, Δ, must therefore be large compared to the terms which tend to mix the two manifolds. If the two $S=\tfrac{1}{2}$ subsystems have g tensors $\mathbf{g}_A$ and $\mathbf{g}_B$, the combined spin Hamiltonian is

$$\mathcal{3C}=\beta\mathbf{H}\cdot\mathbf{g}_A\cdot\mathbf{S}_A+\beta\mathbf{H}\cdot\mathbf{g}_B\cdot\mathbf{S}_B+\Delta\mathbf{S}_A\cdot\mathbf{S}_B$$
$$=\tfrac{1}{2}\beta\mathbf{H}\cdot(\mathbf{g}_A+\mathbf{g}_B)\cdot\mathbf{S}+\tfrac{1}{2}\Delta(S^2-\tfrac{3}{2})$$
$$+\tfrac{1}{2}\beta\mathbf{H}\cdot(\mathbf{g}_A-\mathbf{g}_B)\cdot(\mathbf{S}_A-\mathbf{S}_B),$$

where $\mathbf{S}=\mathbf{S}_A+\mathbf{S}_B$. The first two terms are diagonal in S^2, while the last term, which is purely off-diagonal, constitutes the mixing term. The transition to an unperturbed system of $S=0$ and $S=1$ levels, therefore, occurs when Δ exceeds the *difference* in Zeeman energies. In analogy to a chemical bond, the singlet level should have the lower energy, but the value of Δ required to give a pure $S=1$ spin Hamiltonian is so small that the occurrence of fully populated triplet levels at 77°K is not surprising. The maximum difference in g values we have observed is $\delta g\approx0.01$, giving at K band $\Delta\gg\beta H\delta g$

TABLE V. The comparison of centers (II,III), Si-B,[a] Si-C,[a] and Si-J.[a] (g_1 and g_3 for center (II,III) are interchanged to agree with the nomenclature of Watkins and Corbett.)

Centers	g_1[b]	g_2	g_3	θ'[c] (deg)	A_{II} (10^{-4} cm^{-1})	$A_\perp$ (10^{-4} cm^{-1})	hfs axis[e]
(II,III)	2.0009	2.0099	2.0102	0.9±0.2	68.8±0.4	43.9±0.4	$-1.2°$
Si-B	2.0026	2.0085	2.0107	1.3±0.7	130 ±2	71 ±2	⟨111⟩
Si-C	2.0012	2.0135	2.0150	6 ±1	79 ±2	56 ±2	⟨111⟩
Si-J	2.0004	2.0020	2.0041	7.7±0.5	67.8±0.05	40.5±0.5	⟨111⟩

Centers	a (10^{-4} cm^{-1})	b (10^{-4} cm^{-1})	α^2	β^2	η^2	% w.f.[d]
(II,III)	-52.2	-8.3	0.176	0.824	0.281	56
Si-B	-91	-20	0.14	0.86	0.64	64
Si-C	-64	-27	0.22	0.78	0.28	56
Si-J	-49.3	-9.3	0.16	0.84	0.31	62

[a] The Si-B, C, and J center data are taken from Watkins and Corbett (see Refs. 7 and 8).
[b] $g = \pm0.0001$ for (II,III) and ±0.0003 for others.
[c] Angle of g_1 axis from $\langle\bar{1}11\rangle$ towards $\langle\bar{1}10\rangle$. Note that $\theta' = 35.3° - \theta$.
[d] Fraction of the wave function localized on the central atoms.
[e] Angle of hfs from $\langle\bar{1}11\rangle$ towards $\langle\bar{1}10\rangle$.

$\approx 5\times10^{-7}$ eV, or 0.006°K. The low-temperature data indicate that center (V,VI) and perhaps center (II,III) are depopulated at 4.2°K, indicating that Δ, in fact, lies between 4.2 and 77°K. The low temperature behavior of centers (I,I') and (VI,VII) is unknown. We have not seen any indication of the forbidden transitions or second order hfs effects which should arise for small values of Δ, nor of the perturbations arising when one of the triplet levels crosses the singlet.

The above discussion shows the g tensor observed in the triplet manifold to be the average of those belonging to the two subsystems: $\mathbf{g} = \frac{1}{2}(\mathbf{g}_A + \mathbf{g}_B)$. The interaction of the two systems will also displace the energies of the excited levels involved in the g shifts by amounts presumably of the same order of magnitude as Δ, and the g shifts will undergo a fractional change of order $\bar{\Delta}/\bar{E}$, where $\bar{E}$ is the average excitation energy of these levels. Taking $\bar{E}\approx1$ eV [20] and $\Delta<0.0064$ eV (i.e., 77°K), the fractional change in g shift is only 0.6%. In this light, the following observations are suggestive: (1) the g tensors of centers (II,III) and (I,I') are nearly axially symmetric along a $\langle111\rangle$ axis with a relatively small g shift in this direction: This is consistent with a pair of parallel or antiparallel $\langle111\rangle$ dangling bonds. (2) The g tensors of centers (V,VI) and (VII,VIII) can be closely approximated by assuming a pair of the above bonds oriented toward the center of a tetrahedron: The ratio of g shifts is very close to 1:2:3 as expected for such a configuration. The relations among these tensors can be seen most clearly by expressing the g-shift tensors, $\delta\mathbf{g} = \mathbf{g} - g_0\mathbf{1}$, in the crystalline coordinate system. A $\langle111\rangle$ axially symmetric tensor having $\delta g_3 = 0$ has only one independent parameter and takes the form $\boldsymbol{\delta}_1$ below, while the average of two such tensors whose principal axes are $\langle111\rangle$ and $\langle\bar{1}\bar{1}1\rangle$—i.e., which make a tetrahedral or octahedral angle with each other—takes

the form $\boldsymbol{\delta}_2$. The elements below the diagonal are redundant and have been suppressed.

$$\boldsymbol{\delta}_1 = \begin{pmatrix} \delta & -\frac{1}{2}\delta & -\frac{1}{2}\delta \\ & \delta & -\frac{1}{2}\delta \\ & & \delta \end{pmatrix}, \quad \boldsymbol{\delta}_2 = \begin{pmatrix} \delta & -\frac{1}{2}\delta & 0 \\ & \delta & 0 \\ & & \delta \end{pmatrix}.$$

These are seen to be satisfactory representations of the observed g-shift tensors:

Type 1:

$$(\text{I,I'}): \quad \delta\mathbf{g} = \begin{pmatrix} 0.0048_1 & -0.0020_2 & -0.0025_8 \\ & 0.0048_1 & -0.0025_8 \\ & & 0.0048_3 \end{pmatrix},$$

$$(\text{II,III}): \quad \delta\mathbf{g} = \begin{pmatrix} 0.0046_3 & -0.0030_3 & -0.0030_4 \\ & 0.0046_3 & -0.0030_4 \\ & & 0.0049_5 \end{pmatrix};$$

Type 2:

$$(\text{V,VI}): \quad \delta\mathbf{g} = \begin{pmatrix} 0.0043_5 & -0.0023_4 & -0.0001_2 \\ & 0.0043_5 & -0.0001_2 \\ & & 0.0047_5 \end{pmatrix},$$

$$(\text{VII,VIII}): \quad \delta\mathbf{g} = \begin{pmatrix} 0.0047_6 & -0.0019_5 & 0 \\ & 0.0047_6 & 0 \\ & & 0.0049_4 \end{pmatrix};$$

and we conclude that the four centers are made up from one basic unit, the dangling sp^3 orbital.

An important feature of this model is the sensitivity of the zero-field splitting to the geometry of the two orbitals. Even minor variations in their relative positions would smear out the EPR spectra. It seems unlikely that these sharply defined defects can be closely associated with damage of the type observed in fast-neutron-irradiated germanium, where large regions of apparent disorder have been observed in electron micrographs.[21]

[20] G. D. Watkins and J. W. Corbett deduce an $\bar{E}$ of 2.5 eV for the Si-A center.

[21] J. R. Parsons, R. W. Balluffi, and J. S. Koehler, Appl. Phys. Letters 1, 57 (1962).

B. Discussion of Center (II,III)

Although there has been no direct correspondence between the EPR centers observed in neutron-irradiated and electron-irradiated silicon, primarily because of the difference in Fermi levels of the samples studied, there are remarkable similarities between the spin-Hamiltonian parameters of the centers. To facilitate comparison, the g and A tensors, and the values of α^2, β^2, and η^2 for centers (II,III), Si-B, Si-C, and Si-J are collected in Table V. The Si-B center is one of a class which is believed to arise from an electron concentrated in an isolated, but slightly distorted dangling bond orbital. It is found in both p- and n-type electron-irradiated samples. The Si-C and Si-J centers are believed to be two different charge states of a divacancy; the Si-C center being found in high resistivity n- and p-type samples, the Si-J center in p type.

Table V shows that (1) the over all symmetry of center (II,III) reflected by the g tensor is similar to the Si-B center, suggesting a pair of parallel or antiparallel $\langle 111 \rangle$ dangling bonds; (2) the magnitude of the A tensor is comparable to those for the Si-C and Si-J centers, indicating a similar configuration of electron clouds over two equivalent nuclei; and (3) the fractional s character of the center (II,III) orbital is appreciably less than that of the Si-C center, which is presumably in an antibonding state, and slightly more than that of the Si-J center, which is bonding. As the defect of s character (from 25%) is a measure of the relaxation of the atoms back along the axis of the broken bond, this observation is compatible with very weak bonding of the two electrons in center (II,III). Unfortunately, the even lower s character of the Si-B center reduces the force of the argument. Implicit in Table V is the exact equivalence of the two central nuclei of center (II,III), as shown by the lack of splitting of the hyperfine lines (Fig. 2). This equivalence despite the slight distortion of the hfs axis away from $\langle 111 \rangle$ suggests that the dangling bonds involved are antiparallel. A similar comparison of the Si-B center and the N center at 77°K is discussed by Nisenoff and Fan.[2]

The fact that a divacancy originally has two sets of three broken bonds makes it easy to visualize two unbridged and unpaired electrons forming a spin-1 system in the neutral charge state, permitting speculation that center (II,III) is the neutral charge state of the divacancy. The divacancy model of center (II,III) however, appears to be incompatible with the work of Watkins and Corbett[8] on the following grounds: (1) while the Si-C and Si-J centers are stable up to 300°C, center (II,III) anneals out at 185°C: and (2) the motional broadening effect observed above 77°K for the Si-J center is absent for center (II,III). The lower annealing temperature indicates that it is less stable, while the absence of the motional effect suggests an additional mechanism which locks the electronic configuration more firmly and make the averaging motion

more difficult. The approximate value of 10 for the number of next-nearest neighbors argues that center (II,III) is not too dissimilar to a divacancy.

The distinct $\langle 111 \rangle$ axial symmetry of the g and A tensors of center (II,III) thus strongly supports the picture of a pair of electrons localized in antiparallel dangling bond orbitals aligned in a $\langle 111 \rangle$ direction. The nearly axial $\langle 111 \rangle$ symmetry of the D tensor suggests that the two electronic spins are separated along a direction very close to $\langle 110 \rangle$ by a well-defined distance of the order of a lattice spacing, or 5 Å.

Although we lack detailed information on the A tensors of the other spin-1 centers, it is tempting to suppose that they are related to center (II,III) by the addition of oxygen bridges analogous to that of the Si-A center and are responsible for the satellites observed by Ramdas and Fan[22] on the 11.98-μ infrared absorption band in neutron-irradiated crucible silicon.

ACKNOWLEDGMENTS

APPENDIX

The eigenvalues and transition frequencies usually derived for the Hamiltonian

$$\mathcal{3C} = \beta \mathbf{H} \cdot \mathbf{g} \cdot \mathbf{S} + \mathbf{S} \cdot \mathbf{D} \cdot \mathbf{S}$$

assume the axes of $\mathbf{g}$ and $\mathbf{D}$ to coincide. By treating the zero-field splitting term as a perturbation, we here derive invariant expressions which are valid through second order of $D_e/g_e\beta H$ for all values of S and for $\mathbf{g}$ and $\mathbf{D}$ having arbitrary axes. Without loss of generality, we take $\mathbf{g}$ and $\mathbf{D}$ to be symmetric and set trace $\mathbf{D}=0$.

Choosing the coordinate system in such a way that $\mathbf{k}$, a unit vector along the z axis, lies along the effective magnetic field, i.e., $\mathbf{g} \cdot \mathbf{H} = g_e H \mathbf{k}$, and working in the representation in which S and S_z are diagonal, the energy levels up to the second order are given by

$$E_m = \beta g_e H \langle m | S_z | m \rangle + \langle m | \mathbf{S} \cdot \mathbf{D} \cdot \mathbf{S} | m \rangle$$
$$+ \sum_{m'}{}' \frac{\langle m | \mathbf{S} \cdot \mathbf{D} \cdot \mathbf{S} | m' \rangle \langle m' | \mathbf{S} \cdot \mathbf{D} \cdot \mathbf{S} | m \rangle}{E_m - E_{m'}},$$

where

$$g_e = (\mathbf{H} \cdot \mathbf{g}^2 \cdot \mathbf{H})^{1/2}/H.$$

---

[22] A. K. Ramdas and H. Y. Fan, in *International Conference on Crystal Lattice Defects*, Suppl. J. Phys. Soc. Japan 18, 33 (1963).

The quantity $\mathbf{S}\cdot\mathbf{D}\cdot\mathbf{S}$ can be reduced to the form

$$\mathbf{S}\cdot\mathbf{D}\cdot\mathbf{S}=\tfrac{1}{2}(\mathrm{tr}\mathbf{D})(S^2-S_z^2)+D_{zz}(\tfrac{3}{2}S_z^2-\tfrac{1}{2}S^2) \quad (\Delta m=0)$$
$$+\tfrac{1}{2}(D_{zx}-iD_{zy})(S_zS_++S_+S_z)$$
$$+\tfrac{1}{2}(D_{zx}+iD_{zy})(S_zS_-+S_-S_z) \quad (\Delta m=\pm1)$$
$$+\tfrac{1}{4}(D_{xx}-D_{yy}-2iD_{xy})S_+^2$$
$$+\tfrac{1}{4}(D_{xx}-D_{yy}+2iD_{xy})S_-^2, \quad (\Delta m=\pm2)$$

with

$$S_+=(S_x+iS_y), \quad S_-=(S_x-iS_y), \quad \text{and} \quad D_{ij}=D_{ji}.$$

In this form the matrix elements can be easily evaluated and summed to give

$$E_m=mg_e\beta H+\tfrac{1}{2}[3m^2-S(S+1)]D_{zz}$$
$$+\tfrac{1}{2}[S(S+1)-m^2](\mathrm{tr}\mathbf{D})$$
$$-\tfrac{1}{2}(g_e\beta H)^{-1}m[4S(S+1)-8m^2-1](D_{zx}^2+D_{zy}^2)$$
$$+\tfrac{1}{8}(g_e\beta H)^{-1}m[2S(S+1)-2m^2-1]$$
$$\times[(D_{xx}-D_{yy})^2+4D_{xy}^2].$$

In invariant form, after setting $\mathrm{tr}\mathbf{D}=\sum_i D_{ii}$ equal to

zero, with $D_e=\mathbf{k}\cdot\mathbf{D}\cdot\mathbf{k}$ and $\mathrm{tr}\mathbf{D}^2=\sum_{ij}D_{ij}^2$, one has

$$E_m=mg_e\beta H+\tfrac{1}{2}[3m^2-S(S+1)]D_e$$
$$+(g_e\beta H)^{-1}m\{\tfrac{1}{4}[2S(S+1)-2m^2-1](\mathrm{tr}\mathbf{D}^2)$$
$$-[3S(S+1)-5m^2-1](\mathbf{k}\cdot\mathbf{D}^2\cdot\mathbf{k})$$
$$+\tfrac{1}{8}[18S(S+1)-34m^2-5]D_e^2\}.$$

The transition $m\leftrightarrow m+1$ will occur at the frequency given by

$$h\nu_m=E_{m+1}-E_m$$
$$=g_e\beta H+\tfrac{3}{2}(2m+1)D_e$$
$$+(g_e\beta H)^{-1}\{\tfrac{1}{4}[2S(S+1)-6m(m+1)-3](\mathrm{tr}\mathbf{D}^2)$$
$$-[3S(S+1)-15m(m+1)-6](\mathbf{k}\cdot\mathbf{D}^2\cdot\mathbf{k})$$
$$+\tfrac{1}{8}[18S(S+1)-102m(m+1)-39]D_e^2\}.$$

For $S=1$, the expressions for the transition frequencies reduce to

$$m=0 \text{ to } \pm1: \quad h\nu_\pm=g_e\beta H\pm\tfrac{3}{2}D_e$$
$$+(4g_e\beta H)^{-1}(\mathrm{tr}\mathbf{D}^2-\tfrac{3}{2}D_e^2).$$